

Highly nonlinear sub-micron silicon nitride trench waveguide coated with gold nanoparticles

Yuewang Huang^a, Qiancheng Zhao^a, Nicholas Sharac^b, Regina Ragan^b and Ozdal Boyraz^{*a}

^aDepartment of Electrical Engineering and Computer Science, University of California-Irvine, Irvine, CA, USA 92697;

^bDepartment of Chemical Engineering and Materials Science, University of California-Irvine, Irvine, CA, USA 92697

ABSTRACT

We demonstrate the fabrication of a highly nonlinear sub-micron silicon nitride trench waveguide coated with gold nanoparticles for plasmonic enhancement. The average enhancement effect is evaluated by measuring the spectral broadening effect caused by self-phase-modulation. The nonlinear refractive index n_2 was measured to be 7.0917×10^{-19} m²/W for a waveguide whose W_{open} is 5 μ m. Several waveguides at different locations on one wafer were measured in order to take the randomness of the nanoparticle distribution into consideration. The largest enhancement is measured to be as high as 10 times. Fabrication of this waveguide started with a MEMS grade photomask. By using conventional optical lithography, the wide linewidth was transferred to a <100> wafer. Then the wafer was etched anisotropically by potassium hydroxide (KOH) to engrave trapezoidal trenches with an angle of 54.7°. Side wall roughness was mitigated by KOH etching and thermal oxidation that was used to generate a buffer layer for silicon nitride waveguide. The guiding material silicon nitride was then deposited by low pressure chemical vapor deposition. The waveguide was then patterned with a chemical template, with 20 nm gold particles being chemically attached to the functionalized poly(methyl methacrylate) domains. Since the particles attached only to the PMMA domains, they were confined to localized regions, therefore forcing the nanoparticles into clusters of various numbers and geometries. Experiments reveal that the waveguide has negligible nonlinear absorption loss, and its nonlinear refractive index can be greatly enhanced by gold nano clusters. The silicon nitride trench waveguide has large nonlinear refractive index, rendering itself promising for nonlinear applications.

Keywords: silicon nitride trench waveguide, sub-micron, gold nanoparticles, nonlinearity, plasmonic enhancement.

1. INTRODUCTION

Nonlinear fiber optics plays a significant role in supercontinuum generation, all-optical switching, Raman applications and etc. Its mechanism has been thoroughly studied [1] and its application are vastly investigated. Nonlinear properties in waveguides can be engineered through waveguide design, and the concepts been applied to silicon waveguides have flourished integrated silicon photonics towards all-silicon-solution since the first demonstration of a silicon Raman laser [2]. However in telecommunication frequency range, the relatively small energy bandgap of silicon results in inevitable loss due to two photon absorption (TPA) [3]. Alternative materials were explored to mitigate the nonlinear losses while at the same time increase nonlinear response. Silicon nitride draws the attention because of the absence of TPA and free-carrier absorption [4] as an alternative to silicon in nonlinear applications[5]. Its nonlinear refractive index n_2 was measured to be 2.4×10^{-15} cm²/W [6] for the first time. Besides, silicon nitride has a broad transparency windows ranging from the visible to the mid-infrared. The moderate refractive index difference between silicon nitride and silicon dioxide, $\Delta n \approx 0.55$, makes the silicon nitride waveguide with silicon dioxide cladding suitable for low loss propagation [7]. On the fabrication side, silicon nitride can be deposited by standard CMOS fabrication technology, and experiments has already proven that silicon nitride, silicon dioxide and silicon components can be all integrated in one photonic device [8]. Recently we demonstrated a sub-micron silicon nitride trench waveguide using conventional photolithography with low propagation loss and high nonlinearity [9], [10]. The fabricated waveguide has an impressive nonlinear refractive index $n_2 = 1.39 \times 10^{-19}$ m²/W.

To further increase the nonlinear response of the waveguides, plasmonic effect can be used. Such effects arise from coherent oscillations of conduction electrons near the surface on noble metal structures. Carefully designed structures provide field enhancement near the metal-dielectric interface. Among the vastly investigated metal structures, nanoparticles and nanoclusters are widely used in medical diagnostics [11], solar cells [12], [13], surface-enhanced Raman scattering sensors [14], [15] and etc. Fabrication of self-organized clusters of metal particles are developing towards low-cost and highly reproducible ways [16]. For metal nanoparticles, the enhancement associated with the excitation of localized surface plasmons (LSPs). Localized surface plasmons results from plasma oscillation in confined geometries like nanoparticles, or subwavelength features on a metal surface, e.g., bowtie antennas. The LSP resonance depends on the particle size, shape, spacing and surrounding medium. Since it is confined in a small volume, thereby tremendous enhancement can be achieved near the nanoparticle. The resulting strong fields enhance the nonlinear response locally, which is equivalent to increasing the nonlinearity of a material adjacent to a metal [17]. Experimental studies have shown that noble nanoparticles enhance the optical nonlinearity in nanocomposite films [18], [19] and nanobelts [20].

In this paper, we present the experimental demonstration of the plasmon enhanced optical nonlinearity in sub-micron silicon nitride trench waveguides. Section 2 describes the fabrication procedure of the trench waveguides along with their experimental and numerical characterizations. Section 3 shows the deposition and optical response of the cluster gold nanoparticles using functionalized PMMA templates. Experimental characterization of the third-order nonlinearity of the nanoparticle coated waveguides are illustrated and discussed in Section 4, followed by conclusions in Section 5.

2. SILICON NITRIDE TRENCH WAVEGUIDE

Recently we demonstrated a method to fabricate sub-micron silicon nitride trench waveguide using conventional lithography [9], [10]. The anisotropic potassium hydroxide (KOH) etching on <100> wafer carves a trapezoidal or triangular trench with an angle of 54.7° with respect to the substrate surface, because the etching rate on the <111> direction is extremely slow. The shape of the waveguide is determined by etching time, opening window and silicon nitride deposition thickness. For example, if the etching opening window is smaller than $2 \times \sqrt{2} / 2 \times H$, where H is the etching depth on the silicon substrate, a V-groove will be carved out, and the fabricated waveguide will be in triangle shape. On the contrary, if the etching width is larger than that value, KOH will carve isosceles trapezoidal trench. The width of the lower edge of the waveguide can be estimated as $W = W_{open} - 2 \times \sqrt{2} / 2 \times H$, where W is the width of the lower edge of the waveguide, and W_{open} is the width of the opening window on photo masks. For instance, if the opening window on the photomask is $5 \mu\text{m}$, the lower edge of the etched trenches will be $0.8 \mu\text{m}$, given an etching depth of $3 \mu\text{m}$ in silicon layer.

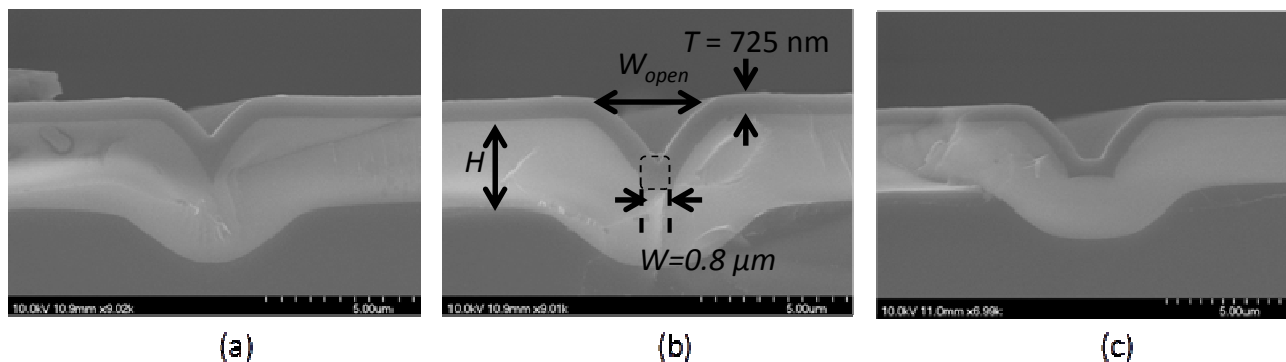


FIG. 1 Fabricated waveguides (a) $W_{open} = 4 \mu\text{m}$, (b) $W_{open} = 5 \mu\text{m}$, and (c) $W_{open} = 6 \mu\text{m}$.

The opening window width and etching depth control the waveguide width, while the thickness of the waveguide is controlled by silicon nitride deposition. Low-pressure-chemical-vapor-deposition (LPCVD) was used to deposit a layer of $T = 725 \text{ nm}$ silicon nitride. The variation of the waveguide geometry affects the waveguide propagation properties and mode distributions, which further influences the nonlinear response of the waveguide. The waveguides propagation losses were experimentally measured using cut-back method for both TE and TM modes [21]. Structure- and polarization-dependent propagation losses were summarized in Table I. We also experimentally tested the nonlinear refractive index n_2 of the guiding material to be $1.39 \times 10^{-19} \text{ m}^2/\text{W}$. In addition, numerical investigation was carried out

using FEM method (COMSOL Multiphysics) to study the effective mode area, dispersion properties and etc. The waveguide with $W_{open} = 5 \mu\text{m}$ was found to have an effective mode area $A_{eff} = 1.9 \mu\text{m}^2$ and a dispersion $D = 55 \text{ ps/nm.km}$. Further details can be found in Ref [9], [10], [21].

Table I Propagation loss of waveguides with different dimensions [21]

	TM	TE
$W_{open} = 4 \mu\text{m}$	$1.66 \pm 0.42 \text{ dB/cm}$	$4.5 \pm 0.34 \text{ dB/cm}$
$W_{open} = 5 \mu\text{m}$	$0.8 \pm 0.26 \text{ dB/cm}$	$3.13 \pm 0.37 \text{ dB/cm}$
$W_{open} = 6 \mu\text{m}$	$6.43 \pm 0.49 \text{ dB/cm}$	$2.95 \pm 0.39 \text{ dB/cm}$

3. GOLD NANOPARTICLE DEPOSITION

Planar assemblies of nanoparticle clusters allow scientists and engineers to harness electromagnetic field enhancements for nonlinear applications, e.g., surface enhanced Raman scattering. Here, gold nanoparticle clusters are assembled onto our waveguides to enhance their nonlinearity. By using a chemical template we can confine metal nanoparticles into tightly spaced clusters in a cheap but robust way, with high throughput [16]. Specifically, a poly(styrene-*b*-methyl methacrylate) (PS-*b*-PMMA) ($M_n = 170\text{-}b\text{-}144 \text{ kg mol}^{-1}$) diblock copolymer is spun coated onto our waveguide, followed by annealing to generate a PS-*b*-PMMA template with lamellar PMMA domains. The PMMA domains are then functionalized with an amine end group, by immersing the substrate in an ethylenediamine/dimethyl sulfoxide (ED/DMSO) solution for 2 hours. 20 nm Au nanoparticles are functionalized with thiotic acid ligands, and an 1-ethyl-3-[3-(dimethylamino)propyl]-carbodiimide hydrochloride/ N-hydroxysulfosuccinimide (EDC/S-NHS) crosslinker is used to facilitate a reaction between the amine group of the PMMA and the carboxylic group on the thiotic acid. Due to the size of the functionalized PMMA domain, which is about 40 nm in width, only a few nanoparticles can be attached to any one domain, resulting in cluster spacings ranging below 7 nm. For the gold nanoparticle attachment, the functionalized PS-*b*-PMMA template is immersed in a solution of functionalized nanoparticles. Previously, two methods have been used. In the first, particles diffuse toward the surface in a gold nanoparticle solution with crosslinker, at 40 °C. An alternative method uses electrophoresis to drive the nanoparticles toward the target. In the diffusion case, cluster spacings between 2 and 7 nm are generated, whereas in the electrophoretic case, spacings smaller than 1 nm were found. In our case, diffusion was used since the silicon nitride is a dielectric material.

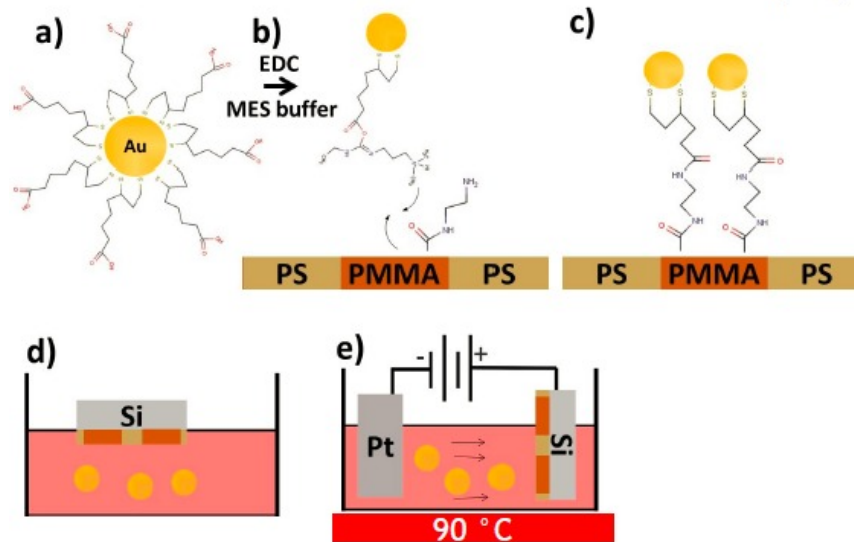


FIG. 2 Gold nanoparticle deposition procedure.

FIG. 3 shows the silicon trench waveguide coated with gold nanoparticle clusters. The nanoparticles are closely packed in the form of dimers, trimers, quadrumers or even hexagonally clusters. The localized surface plasmon strongly relies on the geometries and spacing between the nanoparticles. It can be generalized that discrete clusters (dimers, trimers, and quadrumers) have better field enhancement than hexagonal close packed (HCP) structures. For discrete clusters,

higher cluster numbers and closer spacing are desirable. Detailed simulation results are also available in [16]. Since the nanoparticles are randomly distributed on the waveguides, plasmon enhanced nonlinearity may vary at different locations. Therefore only the average effect of the plasmon enhancement can be detected in a macro scale.

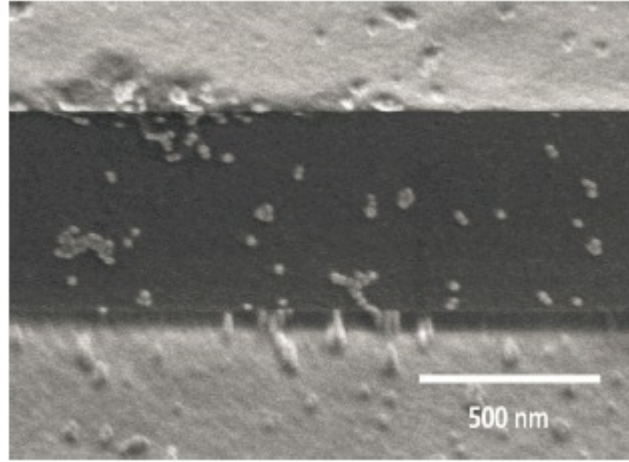


FIG. 3 SEM image of gold nanoparticles deposited on the silicon nitride trench waveguide.

4. NONLINEARITY MEASUREMENT EXPERIMENTS

The nonlinear refractive index n_2 , which is associated with the third order susceptibility of Si_3N_4 was chosen as a figure of merit to characterize the nonlinearity of the waveguide. Spectral broadening caused by self-phase modulation (SPM) of high energy pulses was measured to calculate n_2 [22]. SPM was first observed in 1967 in the context of transient self-focusing of optical pulses propagating in a CS_2 -filled cell [23]. Later systematic studies on SPM in silica-core fiber was done in 1978 [24]. Recently the use of SPM to measure silicon nitride waveguide nonlinearity were frequently presented [10], [25], [26]. In the SPM experiment, ultrafast laser pulses are usually used to provide high peak intensity. Assuming the pulse follows the Gaussian shape, spectral broadening caused by SPM can be theoretically expressed as follows.

$$\Delta\lambda = \Delta\lambda_i + 4\sqrt{\frac{2\ln 2}{e}} \cdot \frac{\lambda_0 n_2 L_{eff}}{c A_{eff}} \cdot \frac{P}{\tau_p} \quad (1)$$

where, $\Delta\lambda_i$ is the spectral width of the input laser pulse, λ_0 is the center wavelength, n_2 is the nonlinear refractive index, L_{eff} is the effective length that is defined as $L_{eff} = (1 - \exp(-\alpha L))/\alpha$ in which α is the propagation loss of the waveguide, and L is the waveguide length, A_{eff} is the effective mode area, P is the peak power and τ_p is the full-width-at-half-maximum (FWHM) of the pulse in time domain. Since the spectral broadening is linearly related to peak power, one can calculate n_2 if the slope of the spectral broadening vs. input power is known. We used a femtosecond pulsed laser (Calmar Laser), $\tau_p = 550$ fs, to provide high intensity source. An attenuator was connected to the pulsed laser to adjust the power. A 50:50 power splitter was used to split the power into the waveguide and an optical power meter (Newport 1830-C) was used to monitor the input power. The light was coupled from fiber to waveguide using a taper-lensed fiber (OZ Optics Ltd). The estimated coupling loss is ~ 7 dB at the input facet. An objective lens (Newport 20X) is placed closely to the waveguide to collect power from waveguide and to collimate the beam so as to be collected by the collimator. An optical spectrum analyzer (ANDO AQ6317B) followed the collimator to analyze the spectrum of the light from the waveguide. The whole experiment setup is illustrated in FIG. 4. The results of two waveguide with $W_{open} = 5 \mu\text{m}$ and $W_{open} = 7 \mu\text{m}$ are shown in FIG. 5.

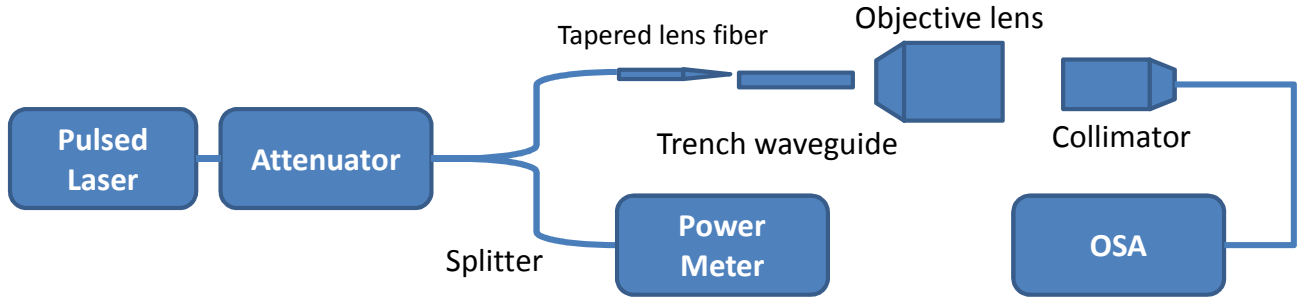


FIG. 4. Experiment setup for characterizing nonlinear refractive index of silicon nitride waveguide.

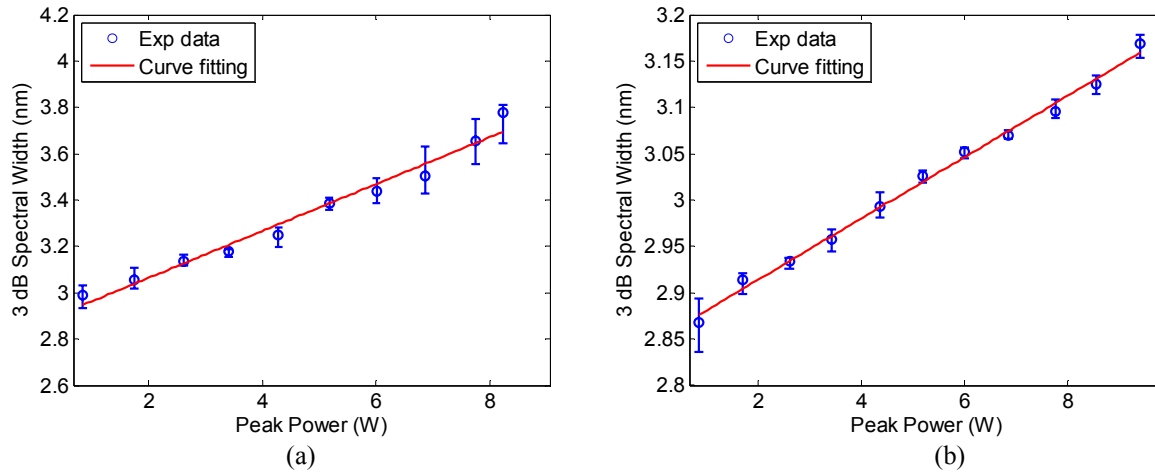


FIG. 5. Spectral broadening as a function of input peak power in waveguide (a) $W_{open} = 5 \mu\text{m}$, and (b) $W_{open} = 7 \mu\text{m}$. The blue error bars are experiment data, each point was measured 10 times. The red line is a linear fitting of the data.

The input peak power is calculated by measuring averaged power. By assuming Gaussian pulses, the peak intensity can be derived as follows.

$$P_0 = 2\sqrt{\frac{\ln 2}{\pi}} \frac{P_{avg}}{\tau_p R} \quad (2)$$

where P_{avg} is the averaged input power, R is the pulse repetition rate. Based on our previous experimental and numerical characterization [9], [10], we assume the propagation loss and effective mode area to be 0.8 dB/cm (TM mode) and $A_{eff} = 1.9 \mu\text{m}^2$ respectively in waveguides with $W_{open} = 5 \mu\text{m}$. Taken the 7 dB coupling loss into consideration, n_2 is calculated as $7.0719 \times 10^{-19} \text{ m}^2/\text{W}$. The group velocity dispersion (GVD) β_2 at $\lambda = 1550 \text{ nm}$ was numerically analyzed to be $701 \text{ fs}^2/\text{cm}$. This value results in a dispersion length $L_D = \tau_p^2/\beta_2 = 431.5 \text{ cm}$, which is much larger than the sample length ($L = 1.12 \text{ cm}$) indicating negligible impact of dispersion at $\lambda = 1550 \text{ nm}$. For waveguide with $W_{open} = 7 \mu\text{m}$, its structure aspect ratio favors TE mode instead of TM mode. Our previous experiments demonstrated that TE mode propagation loss in $W_{open} = 5 \mu\text{m}$ and $W_{open} = 6 \mu\text{m}$ waveguides were 3.13 dB/cm and 2.95 dB/cm, respectively (Table I). The propagation loss in waveguide of $W_{open} = 7 \mu\text{m}$ was calculated using linear extrapolation and estimated to be 2.77 dB/cm. Numerical studies show its effective mode area $A_{eff} = 2.2 \mu\text{m}^2$. Based on these derived parameters, n_2 of the $7 \mu\text{m}$ waveguide is approximately $3.3976 \times 10^{-19} \text{ m}^2/\text{W}$.

Compared to previously reported nonlinear refractive index $n_2 = 1.39 \times 10^{-19} \text{ m}^2/\text{W}$, the measured gold nanoparticles deposited waveguides have an enhancement of 5.09 for $W_{open} = 5 \mu\text{m}$ waveguide and 2.44 for $W_{open} = 7 \mu\text{m}$ waveguide. The enhancement caused by nanoparticle deposition is impressive. However, considering the random distribution of the nanoparticles on the wafer, enhancement may vary at different locations. Therefore a set of waveguides with same structures but at different locations on the wafer were measured and compared. We measured 4 waveguides whose top width $W_{open} = 5 \mu\text{m}$ and two waveguides whose top width $W_{open} = 7 \mu\text{m}$. The samples include waveguides both at the center of the wafer and at the edge, thus are representative for statistics. The measured results are normalized and

compared in FIG. 6. It can be concluded that narrower waveguides ($W_{open} = 5 \mu\text{m}$) have higher nonlinearity than wider waveguides ($W_{open} = 7 \mu\text{m}$) because of smaller effective mode area. The enhancement varies at different groups (locations) indicating the randomness of the nanoparticle distribution. However Group 1 seems to have better enhancement than other groups regardless of the waveguide sizes. The maximum enhancement, which 10 times large, occurs in the waveguide with $W_{open} = 5 \mu\text{m}$ in Group 1.

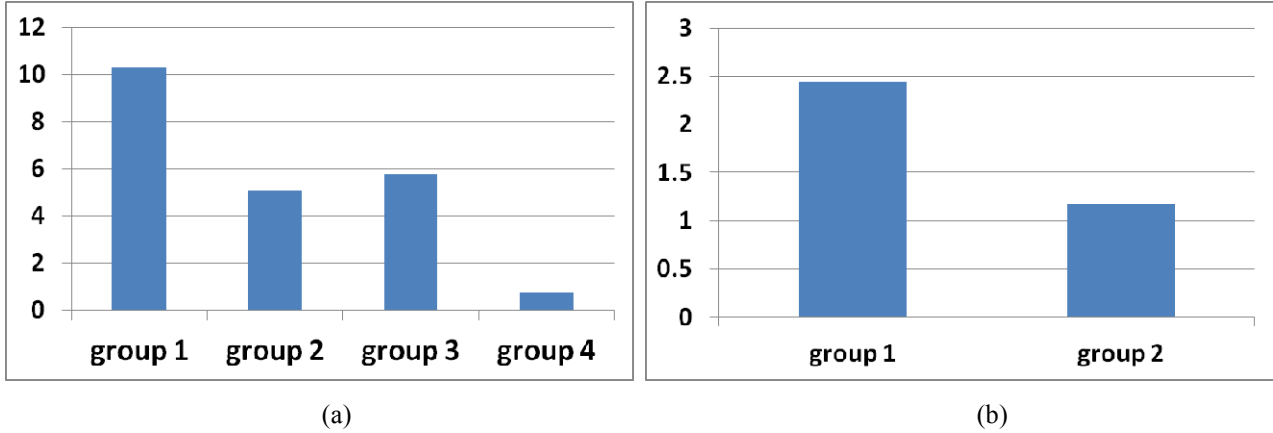


FIG. 6. (a) Enhancement of third-order nonlinearity in waveguides with $W_{open} = 5 \mu\text{m}$. (b) Enhancement of third-order nonlinearity in the waveguides with $W_{open} = 7 \mu\text{m}$.

To further investigate the nonlinear loss of the waveguide, we monitored the power after the attenuator as input power and the power after collimator as output power. A linear relation between the input and output peak power was obtained from a waveguide with $W_{open} = 7 \mu\text{m}$, implying the absence of nonlinear losses. The experiment confirms that TPA should not occur in silicon nitride around $1.55 \mu\text{m}$ because photon energies at this wavelength are less than $E_{g(\text{SiN})}/2$, where the energy bandgap of silicon nitride is $E_{g(\text{SiN})} = 5.3 \text{ eV}$ [25]. To trigger the TPA in silicon nitride, wavelengths must be smaller than 470 nm . This demonstrated linear relation between output power and input power indicates our silicon nitride waveguide is a good candidate in high power nonlinear applications.

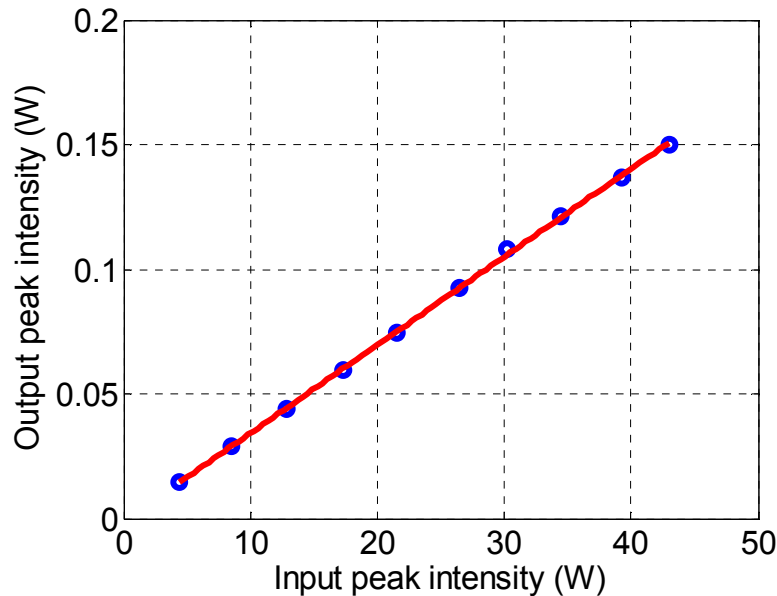


FIG. 7 Measured output peak power vs. input peak power for a silicon nitride trench waveguide with $W_{open} = 7 \mu\text{m}$. The blues circles are measured data while the red curve is a fitting for the data. Input and output losses are counted in the measurement.

5. CONCLUSIONS

In summary, we demonstrated the plasmonic enhanced optical nonlinearity in silicon nitride trench waveguide coated with gold nanoparticles. The average enhancement effect is evaluated by measuring the spectral broadening effect caused by self phase modulation. Several waveguides at different locations on one wafer were measured in order to take the randomness of the nanoparticles into consideration. The waveguide with 5 μm opening width in Group 1 has the largest enhancement, which is almost 10 times. The waveguide exhibits negligible nonlinear loss. Future work may focus on nanoparticle deposition using electrophoresis, and arrayed metal structure for nonlinearity enhancement.

6. ACKNOWLEDGMENT

This work is supported by NSF ECCS 1449397 SNM grant.

REFERENCES

- [1] G. P. Agrawal, *Nonlinear Fiber Optics*. Academic Press, 2007.
- [2] O. Boyraz and B. Jalali, "Demonstration of a silicon Raman laser," *Opt. Express*, vol. 12, no. 21, p. 5269, 2004.
- [3] O. Boyraz, T. Indukuri, and B. Jalali, "Self-phase-modulation induced spectral broadening in silicon waveguides," *Opt. Express*, vol. 12, no. 5, pp. 829–834, Mar. 2004.
- [4] J. S. Levy, A. Gondarenko, M. A. Foster, A. C. Turner-Foster, A. L. Gaeta, and M. Lipson, "CMOS-compatible multiple-wavelength oscillator for on-chip optical interconnects," *Nat. Photonics*, vol. 4, no. 1, pp. 37–40, Jan. 2010.
- [5] D. J. Moss, R. Morandotti, A. L. Gaeta, and M. Lipson, "New CMOS-compatible platforms based on silicon nitride and Hydex for nonlinear optics," *Nat. Photonics*, vol. 7, no. 8, pp. 597–607, Aug. 2013.
- [6] K. Ikeda, R. E. Saperstein, N. Alic, and Y. Fainman, "Thermal and Kerr nonlinear properties of plasma-deposited silicon nitride/ silicon dioxide waveguides," *Opt. Express*, vol. 16, no. 17, p. 12987, Aug. 2008.
- [7] J. F. Bauters, M. J. R. Heck, D. John, D. Dai, M.-C. Tien, J. S. Barton, A. Leinse, R. G. Heideman, D. J. Blumenthal, and J. E. Bowers, "Ultra-low-loss high-aspect-ratio Si₃N₄ waveguides," *Opt. Express*, vol. 19, no. 4, pp. 3163–3174, Feb. 2011.
- [8] Q. Zhao, C. Guclu, Y. Huang, S. Campione, F. Capolino, and O. Boyraz, "Experimental demonstration of directive Si₃N₄ optical leaky wave antennas with semiconductor perturbations at near infrared frequencies," in *Proc. SPIE 9365, Integrated Optics: Devices, Materials, and Technologies XIX*, 2015, vol. 9365, p. 93651K–93651K–10.
- [9] Y. Huang, Q. Zhao, L. Kamyab, A. Rostami, F. Capolino, and O. Boyraz, "Sub-micron silicon nitride waveguide fabrication using conventional optical lithography," in *Advanced Photonics for Communications*, 2014, p. JT3A.27.
- [10] Y. Huang, Q. Zhao, L. Kamyab, A. Rostami, F. Capolino, and O. Boyraz, "Sub-micron silicon nitride waveguide fabrication using conventional optical lithography," *Opt. Express*, vol. 23, no. 5, p. 6780, Mar. 2015.
- [11] A. J. Haes and R. P. V. Duyne, "Preliminary studies and potential applications of localized surface plasmon resonance spectroscopy in medical diagnostics," *Expert Rev. Mol. Diagn.*, vol. 4, no. 4, pp. 527–537, Jul. 2004.
- [12] B. P. Rand, P. Peumans, and S. R. Forrest, "Long-range absorption enhancement in organic tandem thin-film solar cells containing silver nanoclusters," *J. Appl. Phys.*, vol. 96, no. 12, pp. 7519–7526, Dec. 2004.
- [13] S. Pillai, K. R. Catchpole, T. Trupke, and M. A. Green, "Surface plasmon enhanced silicon solar cells," *J. Appl. Phys.*, vol. 101, no. 9, p. 093105, May 2007.
- [14] S. Lal, S. Link, and N. J. Halas, "Nano-optics from sensing to waveguiding," *Nat. Photonics*, vol. 1, no. 11, pp. 641–648, Nov. 2007.
- [15] X.-M. Qian and S. M. Nie, "Single-molecule and single-nanoparticle SERS: from fundamental mechanisms to biomedical applications," *Chem. Soc. Rev.*, vol. 37, no. 5, p. 912, 2008.
- [16] S. M. Adams, S. Campione, J. D. Caldwell, F. J. Bezares, J. C. Culbertson, F. Capolino, and R. Ragan, "Non-lithographic SERS Substrates: Tailoring Surface Chemistry for Au Nanoparticle Cluster Assembly," *Small*, vol. 8, no. 14, pp. 2239–2249, Jul. 2012.
- [17] M. Kauranen and A. V. Zayats, "Nonlinear plasmonics," *Nat. Photonics*, vol. 6, no. 11, pp. 737–748, Nov. 2012.
- [18] sudheesh palengara and C. Keloth, "Metal Nanoparticle Induced Enhancement in Third-Order Optical Nonlinearity of Phenylhydrazone/PMMA thin films," in *International Conference on Fibre Optics and Photonics*, 2012, p. TPo.43.

- [19] V. Singh and P. Aghamkar, "Surface plasmon enhanced third-order optical nonlinearity of Ag nanocomposite film," *Appl. Phys. Lett.*, vol. 104, no. 11, p. 111112, Mar. 2014.
- [20] M. R. Parida, C. Vijayan, C. S. Rout, C. S. S. Sandeep, and R. Philip, "Enhanced optical nonlinearity in β -AgVO₃ nanobelts on decoration with Ag nanoparticles," *Appl. Phys. Lett.*, vol. 100, no. 12, p. 121119, Mar. 2012.
- [21] Y. Huang, *Integrated optical signal processing based on optical waveguides and wavefront-engineered planar devices*. Irvine, Calif: University of California, Irvine, 2014.
- [22] J. Levy, "Integrated Nonlinear Optics In Silicon Nitride Waveguides And Resonators," *PhD Thesis*, Aug. 2011.
- [23] F. Shimizu, "Frequency Broadening in Liquids by a Short Light Pulse," *Phys. Rev. Lett.*, vol. 19, no. 19, pp. 1097–1100, Nov. 1967.
- [24] R. H. Stolen and C. Lin, "Self-phase-modulation in silica optical fibers," *Phys. Rev. A*, vol. 17, no. 4, pp. 1448–1453, Apr. 1978.
- [25] D. T. H. Tan, K. Ikeda, P. C. Sun, and Y. Fainman, "Group velocity dispersion and self phase modulation in silicon nitride waveguides," *Appl. Phys. Lett.*, vol. 96, no. 6, p. 061101, Feb. 2010.
- [26] M.-C. Tien, J. F. Bauters, M. J. R. Heck, D. J. Blumenthal, and J. E. Bowers, "Ultra-low loss Si₃N₄ waveguides with low nonlinearity and high power handling capability," *Opt. Express*, vol. 18, no. 23, p. 23562, Nov. 2010.